JOURNAL OF SPACECRAFT AND ROCKETS
Vol. 47, No. 6, November–December 2010

Deployable Trusses Based on Large Rotation Flexure Hinges

Juan M. Mejia-Ariza*
L'Garde Inc., Tustin, California 92780
and
Thomas W. Murphey† and Hans-Peter Dumm‡
U.S. Air Force Research Laboratory, Albuquerque, New Mexico 87117

DOI: 10.2514/1.48658

Formulations for the strength, stiffness, mass efficiency, and packaging of deployable trusses using flexure hinges are developed and compared with the experiment within. The equations are based on classical buckling theory, Euler buckling with engineering approximations, and finite element-based models to predict the column and bending strengths of solid rod and tubular trusses with slender flexure hinges. Flexure hinge material performance metrics are derived and used to show that, while both mass efficient trusses of solid rods and trusses of tubes are feasible with existing materials, trusses of solid rods are significantly more strain limited. A representative high compaction ratio deployable truss with pultruded carbon fiber reinforced plastic rods and super elastic nickel-titanium alloy flexure hinges was fabricated and tested. The compressive strength of the truss was 48% less than predicted and the compressive stiffness of the truss was 12% less than predicted.

Nomenclature

A	=	cross-sectional area, m^2
c	=	scaling parameter
d	=	strut diameter, m
E	=	Young's modulus, GPa
I	=	cross-sectional moment of inertia, m^4
L	=	length of the hinged strut, m
l	=	half length of strut, m
l_h	=	length of hinge, m
l_r	=	length of strut, m
M	=	bending moment, Nm
m	=	hinged strut mass, kg
n	=	number of longerons
P	=	critical load, N
R	=	radius of the folded hinge, m
R_t	=	truss radius, m
r	=	radius of gyration, m
S	=	slenderness ratio
t	=	thickness of the hinge, m
w	=	width of the hinge, m
x	=	length position of the hinge, m
y	=	deflection, m
β	=	number of truss bays between longeron hinges
γ	=	ratio of the hinge length to the hinged strut length
δ_{mid}	=	deflection at the strut midpoint, m
ε	=	hinge strain
ζ	=	length position of the strut, m
λ	=	eigenvalue
μ	=	longeron structural mass efficiency
ρ	=	density, kg/m^3

Subscripts

b	=	bending loading
c	=	column loading
e	=	effective
h	=	hinge
r	=	strut
l	=	longeron

Received 24 December 2009; revision received 1 July 2010; accepted for publication 25 July 2010.

*Engineer, L'Garde Inc., 15181 Woodlawn Ave. Member AIAA.
†Engineer, Space Vehicles Directorate, 3550 Aberdeen Ave. SE. Senior Member AIAA.
‡Engineer, Space Vehicles Directorate, 3550 Aberdeen Ave. SE.

I. Introduction

DEPLOYABLE trusses conventionally use pin-clevis hinges and ball and socket joints to allow their compact packaging and subsequent deployment in space. An alternative approach is to replace these sliding contact mechanisms with single piece flexure hinges. The large deformations in these flexure hinges require that they are made from larger strain materials while the bulk of the truss can be made from a less flexible, though higher modulus material. This approach, which is shown in Fig. 1, is here called the *concentrated strain approach* and is the focus of this paper.

Several concentrated strain deployable structures have been developed and have demonstrated the feasibility of the approach. For example, Warren reported on an elastically deployed tubular truss with individually articulated axial members. This structure has the features that each bay deploys and locks into place sequentially and the longerons employ midstrut hinges [1]. A patent was also awarded to Warren for a single piece collapsible truss made of foldable tubular members [2]. Murphey analytically showed that efficient deployable trusses based on simple rectangular cross-sectional flexure hinges were possible in [3]. References [4,5] document the design and fabrication of a component of a concentrated strain grillage with trussed elements. The trusses were composed of pultruded carbon fiber reinforced plastic rods and shape memory alloy flexure hinges, similar to the truss reported on herein. The structure was shown to be traceable to a 250:1 linear compaction ratio and high structural mass efficiency. In addition, a truss of tape-springs was developed in [6,7]. The discrete hinges of this truss were formed by structurally thinning the tape-spring laminate in the region of a hinge. Finally, a monolithic articulated concentrated strain elastic structure was developed using tubes with tape-spring hinges [8]. Packaging kinematics for three bays of this truss are shown in Fig. 1.

These previous works did not consider the mechanics of concentrated strain trusses and they limited their scope to point designs or single architectures. As a result, the methods to select an appropriate concentrated strain architecture to meet a given set of requirements were not developed. The purpose of this work is to investigate the structural performance (stiffness, strength, mass efficiency and packaging) of concentrated strain deployable trusses. While concentrated strain architecture trusses that use midstrut

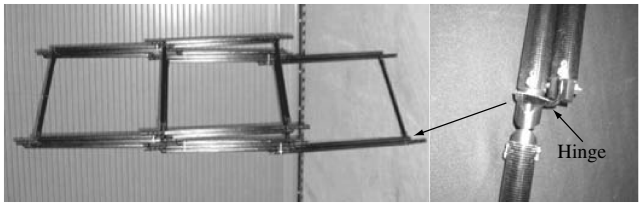

a) Packaged

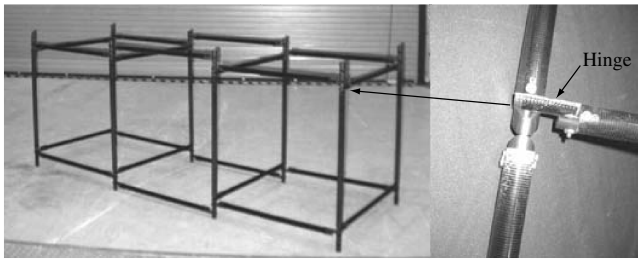

b) Deployed

Fig. 1 Monolithic articulated concentrated strain elastic structure: a) packaged state, and b) deployable state [8].

hinges are conceivable and important, the current work is limited to those with flexure hinges that are located only at the ends of a strut.

The sections of this paper are organized to first understand the axial stiffness and strength behavior of the fundamental concentrated strain truss component: a strut with flexure hinges located on each end (Fig. 2). This element represents a hinged longeron or batten of a builtup truss. A classical buckling analysis of this strut is developed in Sec. II using Euler Column Theory. While accurate, this classical model requires numerical solution and does not yield compact symbolic results. It is used to assess an approximate symbolic model developed in Sec. III. Given the geometry of a hinged strut, these models allow truss strength to be calculated, but they do not consider stiffness or folding of the hinge. Folding failure strain considerations are added to the approximate model of the hinged strut design in Sec. IV. In the remaining sections, truss level considerations are addressed. Strut axial stiffness and ensuing truss bending stiffness are computed in Sec. V. In Sec. VI, truss and material performance metrics are calculated to provide a basis for the selection and development of materials for concentrated strain trusses. Section VII reports on the axial compressive stiffness and strength testing of a concentrated strain deployable truss of solid rods. Finally, results of a finite element analysis of this truss are compared with experimental results in Sec. VIII. Combined, these analyses allow the preliminary design of concentrated strain trusses and provide insight into the impacts of fundamental architecture choices such as strut cross section and hinge material.

II. Classical Model Analysis

Mass efficient trusses have slender struts that, when subjected to a compressive load, typically fail in Euler buckling. If continuous between bays, the longerons buckle into a sinusoidal shape with a period length of two bays [9–11]. In this buckling pattern, the longeron curvature inflection point (point at which there is zero curvature and hence, zero moment), occurs at the longeron-batten interface. Because this is also the location of the flexure hinges, pinned–pinned end conditions best represent a strut buckling failure

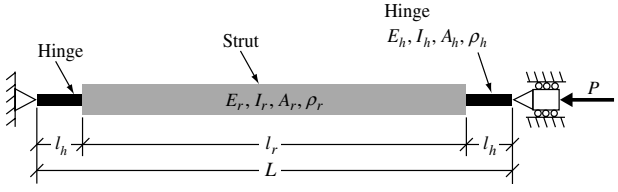

Fig. 2 Simply supported hinged strut.

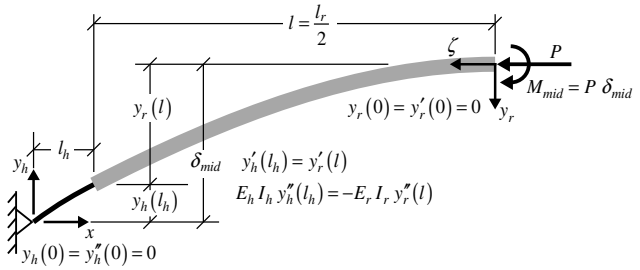

Fig. 3 Classical model buckled configuration nomenclature (transverse deflections exaggerated for clarity).

mode. The compressive strength of such a truss can therefore be predicted with a classical Euler Column Theory model of a hinged strut with pinned–pinned end conditions.

The hinged strut studied in this paper is composed of three piecewise constant cross-sectional segments: a strut with rectangular flexure hinges at both ends, as shown in Fig. 2. Even though the flexure hinges are short compared with the strut segment, the hinges are designed to be slender and fail in buckling when subjected to an axial compressive load. Tape-spring hinges are also promising due to their increased buckling load, however, this slenderness assumption prevents them from being considered here because they fail in non-Euler buckling modes unless sufficiently slender. With these assumptions, an approach similar to that used in [12] is used to determine the critical buckling load and mode shape of the hinged strut. Because the lowest mode is symmetric, only half of the hinged strut is considered for the solution of the eigenvalue problem (Fig. 3).

Using the coordinate systems shown in Fig. 3, the governing differential equations for the hinge and rod segments are

$$y_h'' + \frac{P}{E_h I_h} y_h = 0 \tag{1}$$

$$y_r'' + \frac{P}{E_r I_r} y_r - \frac{P}{E_r I_r} \delta_{\text{mid}} = 0 \tag{2}$$

where δ_{mid} is the total deflection of the midpoint of the strut. The strut coordinate system is fixed to the strut midpoint and moves with transverse deflections. The general solutions of Eqs. (1) and (2) can be written as follows for the two segments of the hinged strut

$$\begin{aligned} &0 \le x \le l_h\text{: } y_h(x) = C_{11}\sin(\lambda_h x) + C_{12}\cos(\lambda_h x) \\ &0 \le \zeta \le l\text{: } y_r(\zeta) = C_{21}\sin(\lambda_r \zeta) + C_{22}\cos(\lambda_r \zeta) + \delta_{\text{mid}} \end{aligned} \tag{3}$$

where λ_h and λ_r are the eigenvalues of the hinge and the strut

$$\lambda_h = \sqrt{\frac{P}{E_h I_h}} \tag{4}$$

$$\lambda_r = \sqrt{\frac{P}{E_r I_r}} \tag{5}$$

The left-end boundary condition for the hinge segment is pinned. In this case, the displacement and the bending moment are zero

$$y_h(0) = y_h''(0) = 0 \tag{6}$$

Application of these to the general solution gives $C_{12} = 0$. The right-end boundary condition for the strut segment is free to sway, but fixed in rotation. In this case, the displacement and slope are zero

$$y_r(0) = y_r'(0) = 0 \tag{7}$$

Application of these to the general solution gives $C_{21} = 0$ and $C_{22} = -\delta_{\text{mid}}$. With these simplifications, the general solutions of Eqs. (1) and (2) are

Table 1 Hinge, strut, and other material properties (composite properties for unidirectional fibers in epoxy matrix at 60% fiber volume fraction unless otherwise noted)

Material	Density, ρ, kg/m^3	Modulus, E, GPa	Failure strain, ε	Strut metric, bending $E^{3/5}/\rho$, N$^{3/5}$m$^{9/5}$/kg	Hinge metric, KPa		
					$E\varepsilon^{1.4}$	$E\varepsilon^{1.7}$	$E\varepsilon^{2.15}$
Torayca M60J carbon fiber composite	1682	354	0.0035	5053	129	23.7	1.86
Hexcel IM7 carbon fiber composite	1594	173	0.01	3470	274	68.9	8.67
Hexcel AS4 carbon fibers in vinyl-ester resin at 58% FVF	1517	130.2	0.01	3075	206	51.8	6.53
AGY S2 glass fiber composite	2000	54	0.02	1375	226	69.8	12.0
spring steel (ASTM A228)	7850	210	0.01	792	333	83.6	10.5
304 stainless steel	8000	193	0.001	738	12.2	1.53	0.068
superelastic nickel-titanium	6450	75	0.037[a]	519	742	276	62.6

[a]Strain used in model; actual strain limit is 0.05.

Table 2 Hinge, strut, diagonal, and truss specifications

Property	Value
Truss length	3.360 m
Truss mass	0.118 kg
Strut length L	140 mm
Truss radius R_t	99.0 mm
Rod material	Hexcel AS4 (Table 1)
Rod area A_r	1.41 ± 0.054 mm^2
Rod diameter d	1.34 ± 0.025 mm
Rod radius of gyration scaling c_l	0.282
Hinge material	Nickel-titanium SMA (Table 1)
Hinge length l_h	6.10 mm
Hinge width w	1.42 mm
Hinge thickness t	0.29 mm
Hinge width scaling factor c_h	2.12
Slenderness S	418
Hinged bay ratio β	12
Hinged to strut length ratio γ	0.0436
Diagonal angle	45 deg.
Diagonal material	304 stainless steel (Table 1) in 1×7 wire rope
Diagonal area	0.05675 mm^2

$$\begin{aligned} &0 \le x \le l_h\text{: } y_h(x) = C_{11}\sin(\lambda_h x) \\ &0 \le \zeta \le l\text{: } y_r(\zeta) = \delta_{\text{mid}}(1-\cos(\lambda_r \zeta)) \end{aligned} \tag{8}$$

Finally, the continuity conditions between hinge and strut segments are

$$y_h'(l_h) = y_r'(l) \tag{9}$$

$$E_h I_h y_h''(l_h) = -E_r I_r y_r''(l) \tag{10}$$

Substituting the general solution into the continuity conditions gives the following system of equations for C_{11} and δ_{mid}

$$\begin{pmatrix} \lambda_h \cos(\lambda_h l_h) & -\lambda_r \sin(\lambda_r l) \\ -E_h I_h \lambda_h^2 \sin(\lambda_h l_h) & E_r I_r \lambda_r^2 \cos(\lambda_r l) \end{pmatrix} \begin{pmatrix} C_{11} \\ \delta_{\text{mid}} \end{pmatrix} = \begin{pmatrix} 0 \\ 0 \end{pmatrix} \tag{11}$$

Setting the determinant of the square matrix on the left side of Eq. (11) equal to zero and simplifying gives an equation for the eigenvalues of the system,

$$\tan(\lambda_h l_h)\tan(\lambda_r l) = \frac{\lambda_h}{\lambda_r} \tag{12}$$

Equation (12) is transcendental and can only be solved numerically. The critical buckling load is the smallest positive numerical solution and corresponds to the first mode shape. The first mode shape for the hinge and strut segments are given by Eq. (8). With δ_{mid} specified, C_{11} can be found by solving the second row of Eq. (11)

$$C_{11} = \delta_{\text{mid}} \frac{\cos(\lambda_r l)}{\sin(\lambda_h l_h)} \tag{13}$$

In subsequent sections, the fabrication and testing of a concentrated strain truss with superelastic nickel-titanium alloy flexure hinges and pultruded carbon fiber reinforce plastic rods is reported on. As an example problem, the classical model is here applied to the hinged strut of this truss. The material properties and dimensions of the hinge and strut are given in Tables 1 and 2 . Loads and deformed shapes for the classical model are given in Table 3 and Fig. 4 to illustrate the lowest load mode shape for three different hinge lengths. These cases differ only in the strut to hinge length ratio, which is varied from a stout hinge to slender hinge. In the first case (stout hinges), only the strut buckles and the critical load is governed by the strut properties. In the third case (slender hinges), only the hinges buckle and the critical load is governed by the hinge properties. In the second case, the strut and hinges buckle in a combined mode and the critical load is determined by a balance between the strut and hinge properties.

III. Approximate Model Analysis

The analysis of the previous section is cumbersome because it involves transcendental equations. In this section, approximations are employed to develop a simpler closed form solution that will form the basis of analyses in subsequent sections. When the hinges or the strut are slender compared with the other, the system buckling load is approximated by the smallest of either the hinge or strut buckling loads. These buckling modes are that of a pinned–pinned strut (Fig. 4, case 1) or that of a pinned–fixed flexure hinge allowing sway (Fig. 4, case 3). By assuming these modes, as shown in Fig. 5, and designing the hinged strut system so that they individually occur at the same load, a balance between the two modes is achieved. An upper bound on the system buckling load can be calculated using compact Euler's Column Formulas for the strut and hinge

Table 3 Buckling loads for three buckling cases: equations

Case	Buckling mode	Hinge length, mm	Equation (15), hinge buckling load, N	Equation (14), strut buckling load, N	Equation (12), system buckling load, N
1	Strut buckles	4.10	31.8	11.7	9.95
2	Strut and hinges buckle	6.10	14.4	12.5	8.57
3	Hinges buckle	8.10	8.14	13.3	6.29

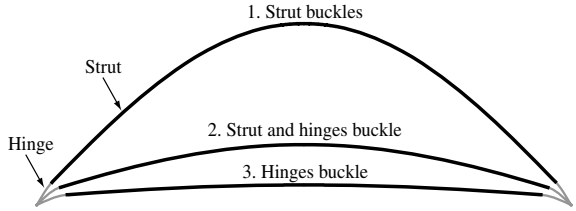

Fig. 4 First mode shape for the three buckling cases of Table 3.

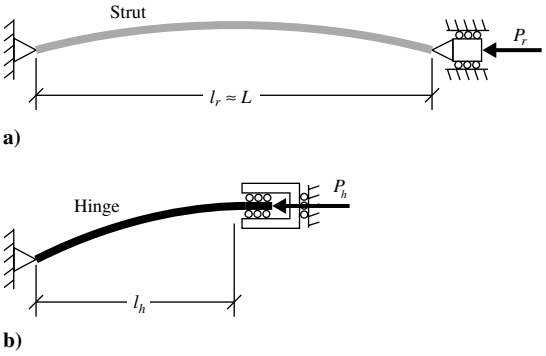

Fig. 5 Approximate model: a) strut, and b) hinge buckling modes and boundary conditions.

$$P_r = \frac{\pi^2 E_r I_r}{l_r^2} \tag{14}$$

$$P_h = \frac{\pi^2 E_h I_h}{4 l_h^2} \tag{15}$$

In this section, these equations will be manipulated to represent the geometry of the hinged strut system and solved for the specific case of both loads being equal.

From Fig. 2, the total hinged strut length is

$$L = l_r + 2l_h \tag{16}$$

Introducing the ratio of hinge length to hinged strut length as γ, the length of the hinge can be written as

$$l_h = \gamma L \tag{17}$$

Substituting Eq. (17) into Eq. (16) and solving for L yields

$$L = \frac{l_r}{1 - 2\gamma} \tag{18}$$

When γ is small, buckling of the strut is approximated by a pinned–pinned strut with length equal to L (Fig. 5a) and the buckling load for the strut is

$$P_r = \frac{\pi^2 E_r I_r}{L^2} \tag{19}$$

It is convenient to express this equation in terms of the strut slenderness (slenderness based on radius of gyration is used here, $S = L/r$) and a parameter that allows the representation of a range of strut cross sections. Solving for the radius of gyration gives

$$r = \frac{L}{S} \tag{20}$$

The strut cross-sectional moment of inertia in terms of radius of gyration and cross-sectional area are,

$$I_r = A_r r^2 \tag{21}$$

Assuming the radius of gyration scales with a constant c_l times the square root of cross sectional area gives,

$$r = c_l \sqrt{A_r} \tag{22}$$

c_l can be calculated from,

$$c_l = \frac{r}{\sqrt{A_r}} = \frac{\sqrt{I_r}}{A_r} \tag{23}$$

and is constant for cross sections that are uniformly scaled. It is 0.282 for a solid rod and 1.995 for a thin wall tube with radius to wall thickness ratio of 50. Solving Eq. (22) for cross-sectional area yields,

$$A_r = \frac{r^2}{c_l^2} \tag{24}$$

Substituting Eqs. (20), (21), and (24) into Eq. (19) gives the strut buckling load in terms of slenderness and c_l,

$$P_r = \frac{\pi^2 E_r L^2}{c_l^2 S^4} \tag{25}$$

Because slenderness and buckling load are directly related with a single equation, they allow a formulation with respect to either one. Solving (25) for slenderness gives,

$$S = \sqrt[4]{\frac{\pi^2 E_r L^2}{c_l^2 P_r}} \tag{26}$$

In the design of efficient truss structures, slenderness often becomes more of a limiting factor than the actual buckling load. For this reason, the current formulation will use slenderness as a variable instead of buckling load.

Assuming the flexure hinge width scales with the strut radius of gyration gives,

$$w = 2c_h r \tag{27}$$

where c_h is 2 for a solid rod with the hinge width equal to the rod diameter and is 1.414 for a thin wall tube. The corresponding hinge cross sectional moment of inertia and the cross sectional area are,

$$I_h = \frac{1}{12} w t^3 \tag{28}$$

$$A_h = wt \tag{29}$$

The critical buckling load of the hinge in terms of strut slenderness is found by substituting Eqs. (17), (20), (27), and (28) into Eq. (15),

$$P_h = \frac{\pi^2 c_h E_h t^3}{24 L S \gamma^2} \tag{30}$$

The premise of the approximate model is that individually the hinge and strut buckle at the same load. The hinge to strut length ratio that assures this happens is found by setting $P_h = P_r$, Eqs. (25) and (30), and solving for γ,

$$\gamma = c_l \sqrt{\frac{c_h E_h S^3 t^3}{24 E_r L^3}} \tag{31}$$

Using the hinge and strut specifications given in Table 2, Eqs. (25) and (30) are plotted in Fig. 6 along with the classical model solution, Eq. (12), as a function of γ. The value of γ when the rod and hinge buckle simultaneously, Eq. (31), is 0.0512 ($l_h = 7.17$ mm). The classical solution for the buckling load is 7.35 N, a nonconservative 29% lower than the approximate solution, 10.38 N. This error tends to decrease with decreasing slenderness and is 32% for a slenderness of 500 and 24% for a slenderness of 300. Consideration of a range of reasonable dimensions showed the error does not exceed 40%. While this error is acceptable for preliminary design or scaling studies, the classical model or finite element models should be used when greater accuracy is needed.

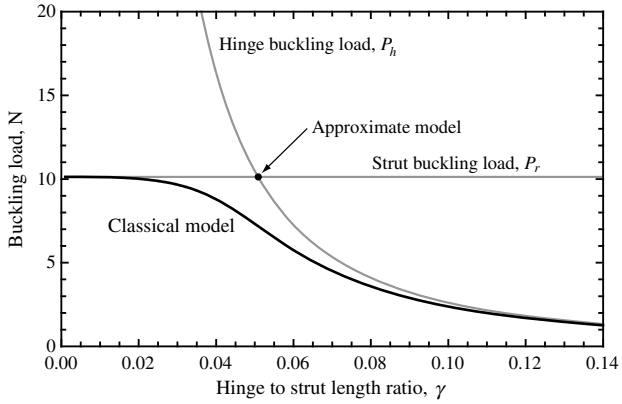

Fig. 6 A comparison between the classical solution and the approximate solution.

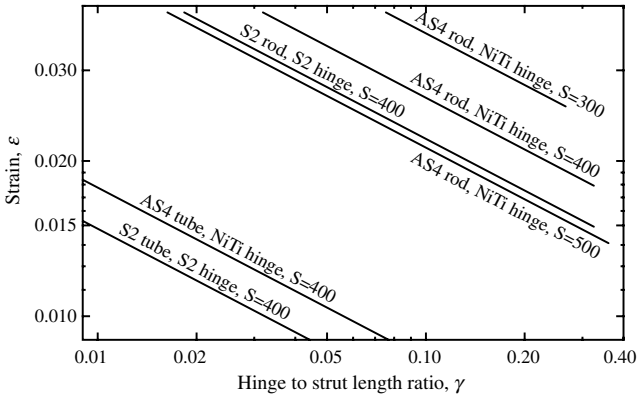

Fig. 8 Hinge strain as a function of hinge to strut length ratio (material properties listed in Table 1).

IV. Strain Limited Design

Flexure hinge strains can severely limit hinge material choices and design freedom. This section extends the approximate model design strategy to include these strains and results in simple equations to estimate and understand the influence of various design choices on the required folding strain.

Figure 7 shows a schematic of the flexure hinge before and after packaging. When the hinged strut is in the stowed configuration, the radius of the folded hinge determines the material strain. Assuming a linear material response, the hinge strain and the length of the folded hinge at 90° are

$$\varepsilon = \frac{t}{2R} \tag{32}$$

$$l_h = \frac{\pi}{2} R \tag{33}$$

Eliminating R from these equations and solving for the flexure thickness gives,

$$t = \frac{4}{\pi} \varepsilon l_h = \frac{4}{\pi} \varepsilon \gamma L \tag{34}$$

Substituting Eq. (34) into Eq. (31) and solving for γ gives the hinge to strut length ratio as a function of hinge strain with the approximate model,

$$\gamma = \frac{3\pi^3 E_r}{8 c_h c_l^2 E_h S^3 \varepsilon^3} \tag{35}$$

and rearranging gives the folding strain as a function of γ,

$$\varepsilon = \frac{\pi}{2S} \left(\frac{3E_r}{c_h c_l^2 \gamma E_h} \right)^{1/3} \tag{36}$$

Similarly, solving Eq. (34) for γ, substituting into Eq. (31) and solving for hinge thickness gives,

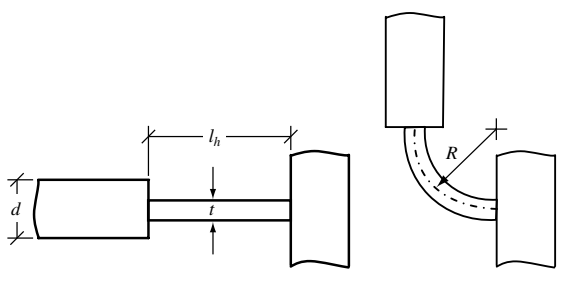

Fig. 7 Schematic of a hinged strut corner: a) deployed configuration, and b) packaged configuration.

$$t = \frac{3\pi^2 E_r L}{2 c_h c_l^2 E_h S^3 \varepsilon^2} \tag{37}$$

Equations (35) and (37) define the geometry of a strain limited hinged strut and can be used for preliminary design along with Eq. (25) for the buckling load.

The equations in this section are valid up to a limited hinge strain because the hinge slenderness decreases below acceptable Euler buckling approximation limits (typically $S > 140$ for a pinned–pinned strut buckling mode or $S > 70$ for the pinned–sway hinge buckling mode). It can be shown that the hinge slenderness is only a function of strain and is given by

$$S_h = \frac{\pi\sqrt{3}}{2\varepsilon} \tag{38}$$

With hinge slenderness limited to 70, strains up to 4% are within the assumptions of this analysis.

Equation (36) shows how the strain required by the concentrated strain approach varies with material and geometry selections. It is graphed in Fig. 8 for a range of hinge and strut specifications. For fixed values of γ, the strain requirement is reduced when the slenderness increases and for a specific slenderness, the strain requirement is reduced as γ increases. From Eq. (36), the strain can also be seen to decrease as strut modulus decreases, hinge modulus increases, or strut hierarchy (c_l) increases. The strain required can be large and modifying these parameters are all appropriate strategies to reducing it. Figure 8 shows the strain requirement is most significantly reduced by using a more hierarchical strut cross section, for example a tubular strut with $R/t = 50$ ($c_l = 1.995$) instead of a solid rod strut ($c_l = 0.282$).

V. Hinged Strut Axial Stiffness

The effective axial stiffness of a hinged strut, $(EA)_e$, is typically reduced in the concentrated strain approach because the hinge modulus and the cross-sectional area are smaller than the strut. This reduces the global buckling load and the bending stiffness of a built-up truss because the truss bending and axial stiffness are directly proportional to the longeron axial stiffness [3],

$$EI = \frac{n}{2} (EA)_e R_l^2 \tag{39}$$

$$EA = n(EA)_e \tag{40}$$

The performance reduction of the hinged strut design can be assessed from the ratio of the effective hinged strut axial stiffness to the stiffness of a strut without hinges, $(EA)_e / E_r A_r$. The effective axial stiffness of the hinged strut system shown in Fig. 2 is obtained by adding the axial stiffness of the strut and two hinges in series,

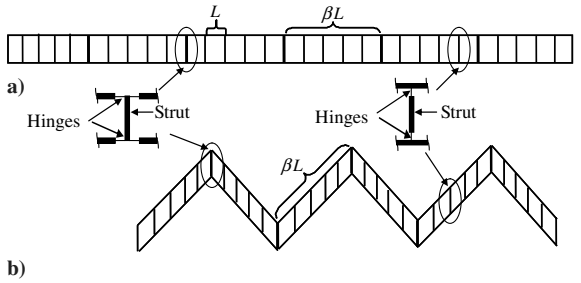

Fig. 9 Shearing truss side view in a) deployed, and b) transitional states.

$$\frac{(EA)_e}{L} = \frac{1}{\frac{2l_h}{E_hA_h} + \frac{l_r}{E_rA_r}} \tag{41}$$

Dividing Eq. (41) by the strut axial stiffness and reorganizing terms gives,

$$\frac{(EA)_e}{E_rA_r} = \frac{2\frac{l_h}{l_r} + 1}{2\frac{l_h}{l_r}\frac{E_rA_r}{E_hA_h} + 1} \tag{42}$$

Equation (42) can be written as a function of γ by solving Eq. (17) for L, substituting into Eq. (16) and solving for l_h/l_r,

$$\frac{l_h}{l_r} = \frac{1}{\frac{1}{\gamma} - 2} \tag{43}$$

The effective hinge to strut length ratio can be much lower when there are less than two hinges per truss bay, as shown in Fig. 9. This deployable truss articulates through longeron z-folding and bay shearing. A longeron is hinged every β truss bays and has an effective length ratio that is β times lower than a single bay, $\gamma_e = \gamma/\beta$, Substituting Eq. (43) into Eq. (42), accounting for the effective length ratio and rearranging terms yields,

$$\frac{(EA)_e}{E_rA_r} = \frac{1}{1 + 2\frac{\gamma}{\beta}(\frac{E_rA_r}{E_hA_h} - 1)} \tag{44}$$

Equation (44) can be written in terms of material properties and design constraints of a strain limited design by substituting in Eqs. (35) and various equations for the hinge and strut cross sections,

$$\frac{(EA)_e}{E_rA_r} = \frac{1}{1 + \pi\frac{E_r}{E_h}(\frac{S^2\varepsilon^2 - 3\pi^2}{4c_hc_l^2S^3\beta\varepsilon^3})} \tag{45}$$

Equation (45) is graphed in Fig. 10 as a function of strain for $\beta = 1$ and $\beta = 12$. The longeron stiffness ratio is highly nonlinear with strain. At smaller strains, the hinge is slender, but relatively thick compared with the strut. At greater strains, the hinge is stout, but relatively thin compared with the strut. This trade between length and thickness creates a nonmonotonic response with strain. In the truss specified in Table 2, the maximum performance reduction is 36% with two flexure hinges per strut ($\beta = 1$). With 12 times fewer hinges per strut ($\beta = 12$, the as-built configuration), a performance reduction of only 4.5% occurs. The performance reduction is also significantly less for tubular struts; it is essentially negligible. Tubes perform better because the change in cross-sectional area between a tube and flexure hinge is much less than the change in area between a solid rod and a flexure.

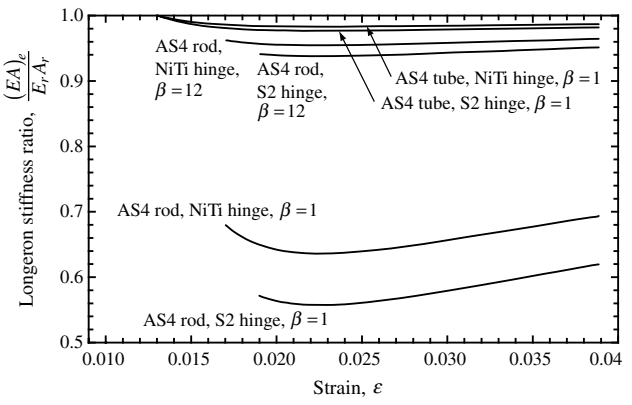

Fig. 10 Effective longeron stiffness and strut axial stiffness ratio vs hinge strain.

VI. Flexure Hinge Material Selection

The balance of hinge properties (modulus, strain and density) best suited to the design of efficient concentrated strain trusses is not immediately obvious. In general, higher modulus, greater strain and lower density all improve efficiency. However, when properties must be traded, for example, increased modulus for reduced strain, the best combination of properties depends on the truss application and the strut properties. In [3], Murphey derived a performance index to assess the structural mass efficiency of longerons in trusses subjected to column (subscript c) and bending (subscript b) loads

$$\mu_c = \frac{P_r^{1/3}(EA)_e^{1/3}L^{5/3}}{\pi^{2/3}m} \tag{46}$$

$$\mu_b = \frac{P_r^{2/5}(EA)_e^{1/5}L^{9/5}}{\pi^{4/5}m} \tag{47}$$

These mass normalized metrics consider longeron buckling load, axial stiffness and total mass and are used here to understand the relationship between hinge material properties and truss performance. Using the strain limited approximate model, the hinged strut buckling load is given by Eq. (25). The effective longeron stiffness is given by Eq. (45) and the mass of the longeron is given by

$$m = L\left(\rho_hA_h\left(\frac{2\gamma}{\beta}\right) + \rho_rA_r\left(1 - \frac{2\gamma}{\beta}\right)\right) \tag{48}$$

where γ is given by Eq. (35). In a strut without hinges, the indices reduce to

$$\mu_c = \frac{(c_lE_r)^{2/3}}{\rho_r} \tag{49}$$

$$\mu_b = \frac{(c_l^4E_r^3)^{1/5}}{\rho_r} \tag{50}$$

Equations (46) and (47) can be normalized by Eqs. (49) and (50) to compare the performance of a truss with hinges to that of an idealized truss without hinges. Doing so allows calculation of the minimum combination of hinge modulus and strain required to achieve a specified level of truss performance reduction. Equations (46) and (47) are normalized and graphed in Figs. 11 and 12 for solid rod and tubular struts and several different strut and hinge material combinations. The solid lines are constant value contours such that the normalized equations evaluate to 0.90 (an arbitrarily chosen approximately 10% mass increase due to hinges). The properties of several potential hinge materials are also plotted as points on the charts. Materials that lie outside (higher and further to the right) of a contour line have a sufficient combination of modulus and strain to allow the architecture with less than a 10% mass increase. Architectures that use materials falling inside of their contour line will incur greater than a 10% mass increase. For these plots, the density of the hinge material has been assumed equal to the strut material. This is not mathematically accurate; however, numerous numerical tests have shown that the results are not highly sensitive to the hinge density.

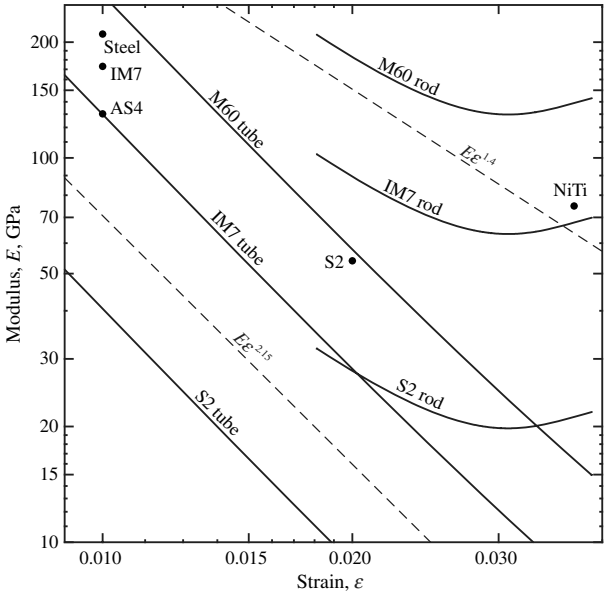

Fig. 11 Hinge material modulus as a function of strain for column loading (contour lines for a 10% performance reduction due to hinges).

Figures 11 and 12 show that efficient (less than a 10% mass penalty) trusses of tubes with flexure hinges made from traditional engineering materials are feasible for all but the stiffest M60J carbon fiber based tubes. With nickel-titanium flexures, these are feasible as well (nickel-titanium can freeze in the packaged configuration and is not able to operate over the broad range of temperatures encountered in space without thermal management). The figures also show that trusses of solid rods require a significantly greater combination of modulus and strain than tubular truss architectures. Efficient trusses of relatively low modulus S2 fiberglass solid rods are feasible with a range of flexure materials. Solid rod trusses of higher modulus (IM7 or M60 carbon fiber composite rods) will incur greater than a 10% mass increase unless space compatible materials with a greater combination of modulus and strain become available.

Attempts to symbolically extract a single material metric from the above equations were unsuccessful. The primary limitation lies in the connection between the hinge requirements and the strut material: it is of diminishing value to have a hinge modulus much greater than the strut modulus. Even so, it can be observed that the contours in Figs. 11 and 12 are linear for tubular truss architectures, suggesting a material metric composed of a product of strain and modulus. Indeed, the parameter $E_h\varepsilon^3$ is observed in both Eqs. (35) and (45) and plays an important role in determining strut performance. As indicated by the dashed lines in the figures, the actual relationship of the contours is approximately $E_h\varepsilon^{2.15}$. (Dashed lines correspond to arbitrarily chosen constant values of the metric that labels the line. Because of the log-log plot scales, these dashed lines are straight and can be parallel offset to achieve greater or lower value contour lines.) Constant values of this metric are nearly parallel to the tubular truss contours for both column and bending applications. For solid rod trusses, this relationship is not nearly as linear, but asymptotes to a constant slope as strain decreases. In the case of column loading, the contours asymptote to $E_h\varepsilon^{1.4}$ and in the case of bending loading, the contours asymptote to $E_h\varepsilon^{1.7}$. These concentrated strain hinge material metrics are listed in Table 1 for several potential hinge materials (greater metric values are better).

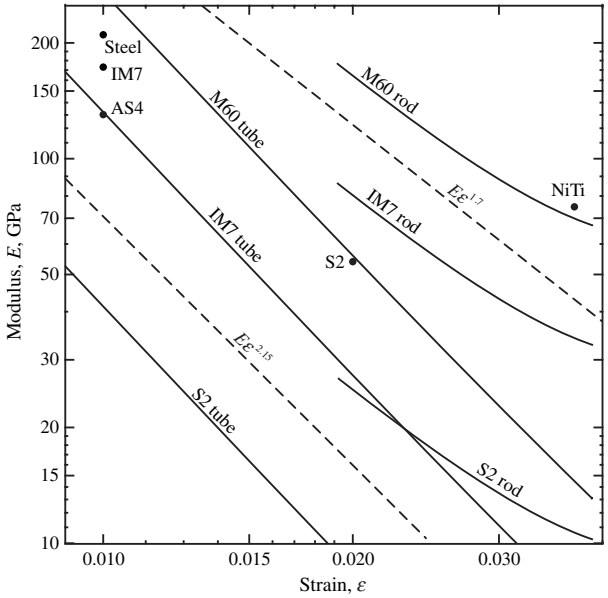

Fig. 12 Hinge material modulus as a function of strain for bending loading (contour lines for a 10% performance reduction due to hinges).

VII. Fabrication and Testing of a Concentrated Strain Truss

A deployable truss of solid rods was fabricated and tested to evaluate the models of the previous sections. Figure 13 shows the truss, which has a total mass of 0.118 kg and length of 3.36 m. The hinges, struts, and diagonals of the truss were connected with three unique joints (shown in Fig. 14) using pin based bonding fixtures to precisely locate components. Materials and dimensions of the truss, strut and hinge are given in Table 2. The truss could serve as a longeron in a hierarchical truss of trusses or as a mast in a blanket solar array or solar sail. The smallest readily fabricated truss dimensions were selected due to the large dimensions arrived at in hierarchical structures. For example, assuming a 50 bay truss of trusses results in a superstructure length of 168 m.

Each truss face was fitted with an extensionally stiff diagonal that goes slack when packaged and a constant force tensioning diagonal that extends by 41% during packaging (Fig. 15). The extendible diagonal design was constructed from 304 stainless steel wire rope and superelastic nickel-titanium ribbon. Diagonals account for 16% of the truss mass. Unloaded, the ribbon is straight. Wire rope is looped through holes in each end of and along the outer surface of the ribbon such that tensioning the wire buckles the ribbon. A wire tension approximately equal to the ribbon buckling load is maintained throughout the extension process. The tension generated by this extendible diagonal is 0.17 N and the diagonals were bonded with this tension applied. For the extensionally stiff diagonal, only the wire rope was used.

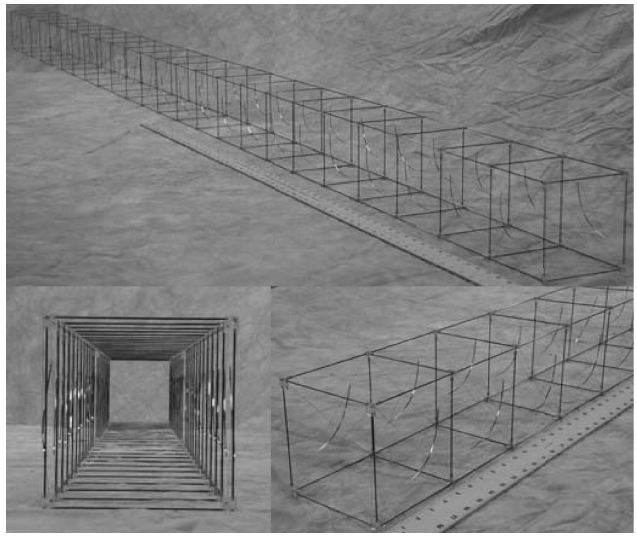

Fig. 13 Concentrated strain deployable truss of solid rods.

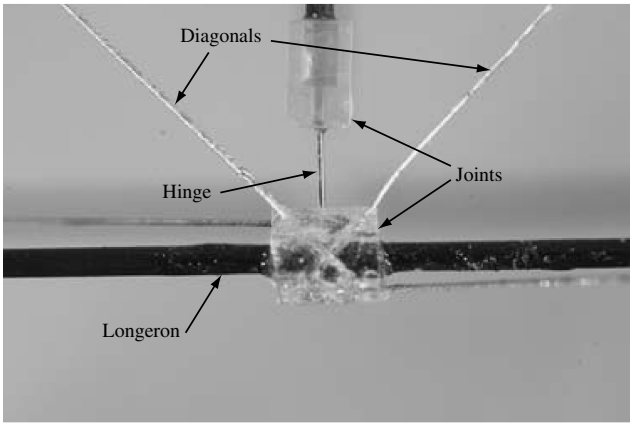

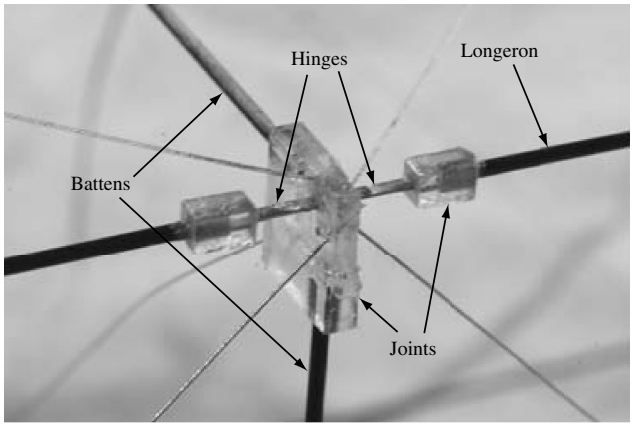

Fig. 14 Rapid prototyped plastic joints and their connectivity.

An axial compressive stiffness and buckling load test was performed on the truss. The displacement and the load on the truss central axis were measured through two effectively rigid plates attached to the truss ends. The plates were fixed to the corners of the truss (longeron ends). The top plate was pinned to an effectively rigid test frame, and the bottom plate was pinned to a load cell. Since the deployable truss could buckle locally or globally and in any direction about its center axis, three sensors per plate (arranged at the vertices of an equilateral triangle centered on the boom) were used to resolve the axial displacement of the two plates, despite potential plate rotation.

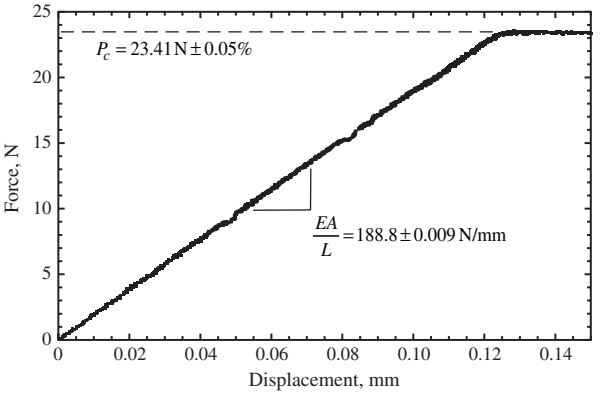

Fig. 16 Buckling test load-displacement data.

Figure 16 shows the load-displacement results of the test and Fig. 17 shows the buckled truss mode shape. Onset of buckling occurred at 22.54 N and plateaued at 23.41 N. The truss buckled locally in two longerons on the top side of the center bay. Linear regression analysis of the data resulted in an axial spring stiffness ($k = EA/L$) of 188.8 N/mm with negligible uncertainty. The load cell used for the test has an uncertainty of $\pm 0.05\%$ of the current load and the displacement sensors have an uncertainty of $\pm 0.1\%$ of the current displacement, both at a 95% confidence level. Based on these uncertainties, the uncertainty in spring stiffness is $\pm 0.1\%$ or ± 0.2 N/mm. The length of the truss is 3.360 m so that the axial stiffness of the truss is $EA = 634,400 \pm 600$ N.

In Fig. 18, the deployable truss is presented in its packaged state with thickness of 25 mm and linear compaction ratio of 1:134.

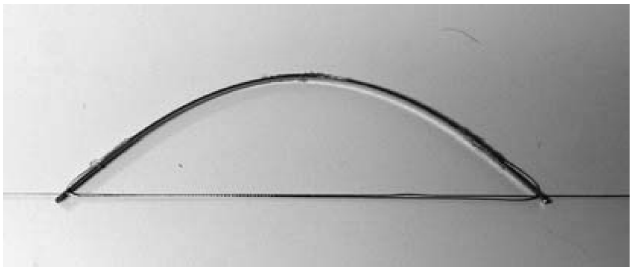

a)

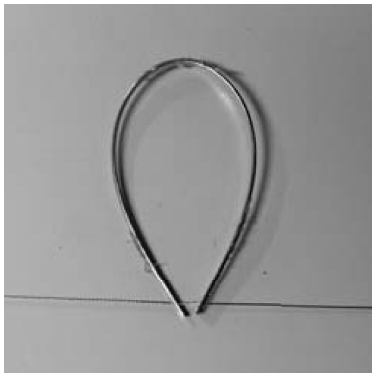

b)

Fig. 15 Extendible diagonal in: a) deployed, and b) packaged configurations.

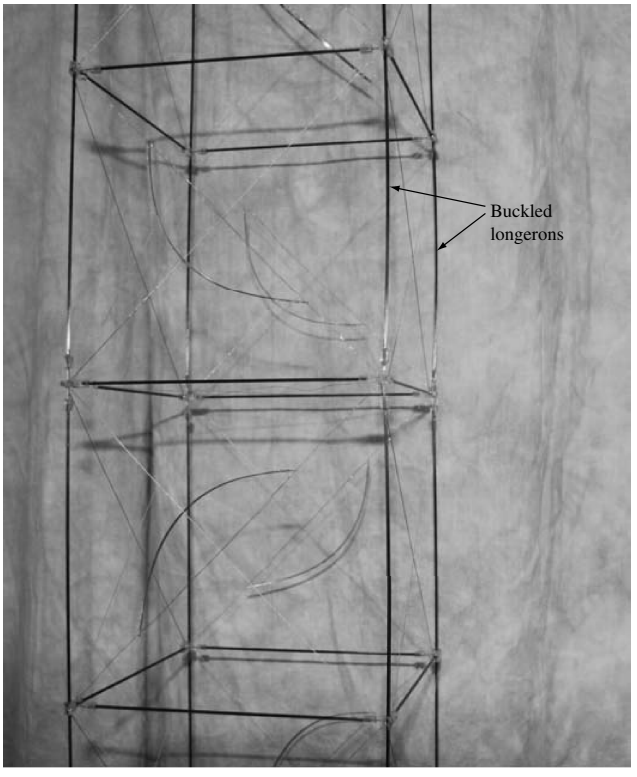

Fig. 17 Buckled truss deformation mode.

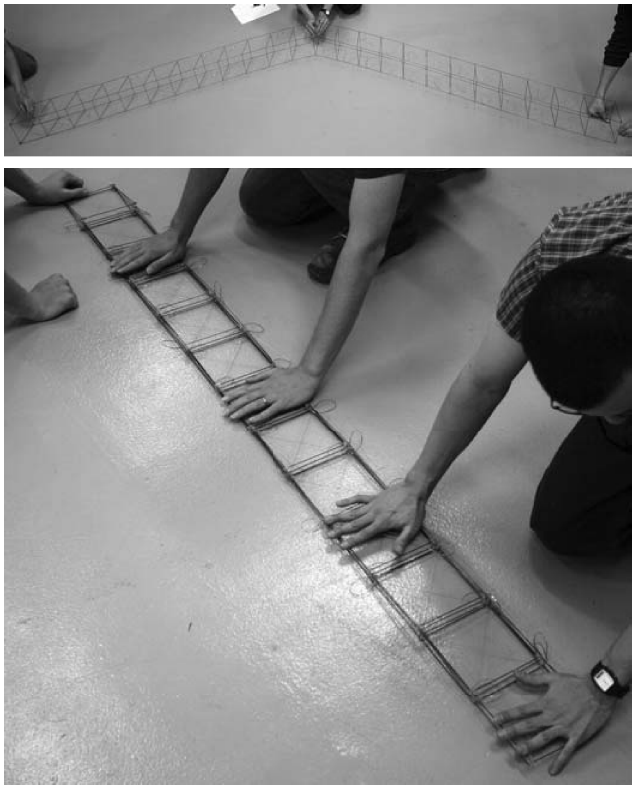

Fig. 18 Deployable truss in the partially and fully packaged states.

VIII. Finite Element Analysis of the Truss

To assess the experimental and analytical model results, a finite element analysis was performed using Abaqus, a general purpose finite element analysis program. Linear perturbation buckling and static load-displacement analyses were carried out with the assumption that the truss was initially straight. The model was constructed entirely from beam elements, except where truss elements were used to model diagonals. Joints that connect parallel rods and hinges were neglected because loads transfer directly from the rod to the hinge. Joints that connect rods and hinges perpendicularly are small and stiff compared with the other elements and were modeled using the strut material and cross section.

Even though the stiff diagonals are incapable of carrying compressive forces, they were modeled as truss elements and carry compressive loads in the analysis. The extensionally soft extendable diagonals were neglected. This method avoids the analysis steps required to model and pretension a soft diagonal and is accurate because the extendable diagonals do not contribute stiffness to the truss.

The ends of the truss were modeled as rigid regions with pinned boundary conditions. This simulated the plates that were attached to the truss. A 1 N load was applied at one end of the truss (the boundary conditions and the load were on the center axis of the truss). The finite element analysis calculated truss axial stiffness is 722,300 N and the first two buckling loads are 44.61 and 44.66 N. Figure 19 shows the buckling modes and it is observed that the longerons buckle into a sinusoidal shape that is either continuous or reverses amplitude through the center batten frame. In the actual truss buckling mode, only two longerons on one side of the truss buckled. This is not surprising since the actual buckling load on each set of longerons is slightly different while the FEA assumes they are identical.

Three different models were used to predict the truss stiffness and buckling load: classical model, approximate model and finite element model. Model predictions and test results are given in Table 4. The approximate and classical predictions are for a single longeron and are multiplied by the number of longerons (four) to give truss results. The approximate predictions represent an idealized truss without hinges (buckling load given by Eq. (19) and axial stiffness given by $E_r A_r$) while the classical predictions account for hinges, Eqs. (12) and (44).

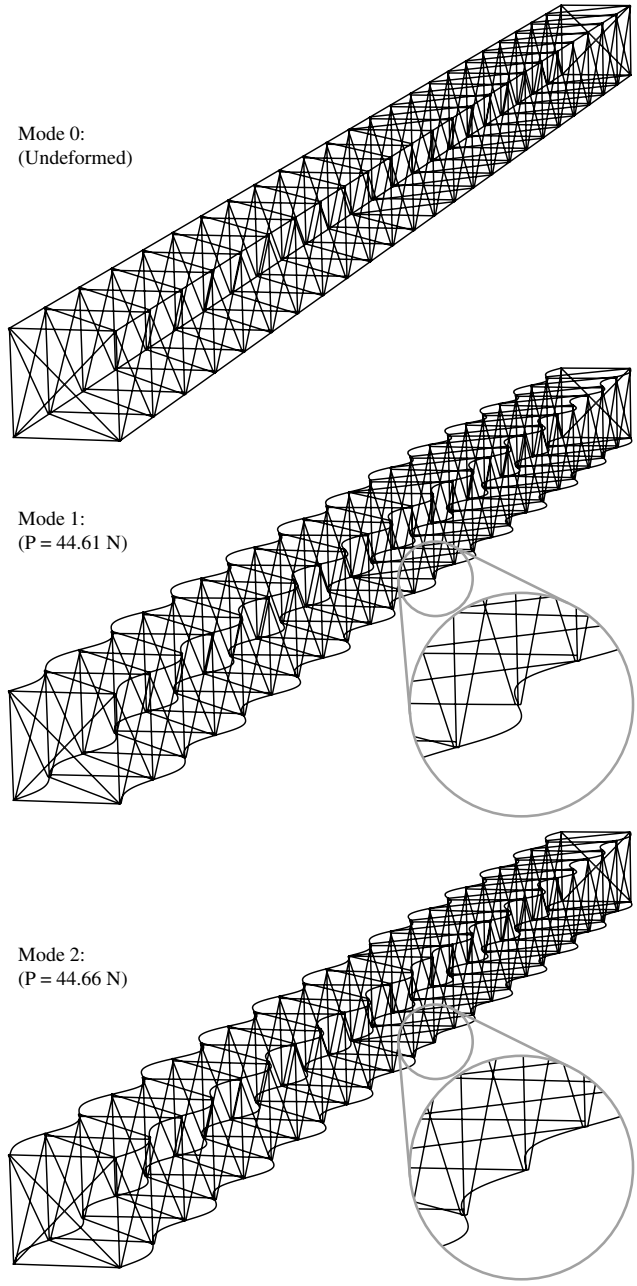

Fig. 19 Buckling load finite element analysis solution (deformations exaggerated).

As expected, the classical analysis buckling load is 17% less than the approximate analysis. It was expected that the finite element analysis would yield a prediction close to the classical analysis; however, it was found that the batten frames add significant rotational stiffness to what the classical model assumes is a pinned connection on the flexure hinges. This added stiffness significantly increases the finite element analysis buckling load. During testing, the truss buckled in the second mode predicted by the finite element analysis. This result is not surprising since the first two modes only differ by 0.1%. However, the experimental buckling load was 48% less than the finite element analysis prediction. This result is attributed to a low diagonal effective stiffness due to insufficient diagonal tension. Close inspection of Fig. 17 shows diagonals that appear to lack tension and that are somewhat wavy. The truss also sheared somewhat during testing. Exercising the finite element model, it was found that reducing the diagonal stiffness by a factor of 340 would result in the observed buckling load. Considering the extremely low

Table 4 Summary of truss analysis and test results

	Approximate	Classical	FEA	Test	% difference
Buckling load, N	41.51	34.26	44.61	23.41	−48
Axial stiffness, N	734,500	709,000	722,300	634,400	−12

initial diagonal tension, this level of stiffness reduction is not unreasonable.

Axial stiffness analysis results are as expected. The classical results reflect a 4.5% stiffness reduction due to hinges. Despite its inclusion of hinges, the finite element model predicts a slight increase in stiffness over the classical model. This is due to two in-extensional diagonals being used on the nonshearing truss faces. These diagonals over constrain the truss and contribute to axial stiffness. Axial stiffness test results were only 12% less than finite element analysis predictions; a difference that is not considered significant, but may be attributed to shear deformations as well as bonded joint stiffness reductions.

IX. Conclusions

Before the work by Warren and Murphey referenced herein, it was not obvious that structurally efficient deployable trusses could be fabricated using flexure hinges. A potential outcome was that readily available flexure materials do not have a sufficient combination of modulus and strain. Through the use of classical analyses, closed form engineering approximations, detailed finite element analysis, fabrication and testing, this paper supports the conclusion that efficient concentrated strain trusses are feasible. Figures 10–12 show that efficient trusses of tubes with flexure hinges made from traditional engineering materials are feasible for all but the stiffest M60J carbon fiber based tubes. With nickel-titanium flexures, these are feasible as well. Efficient trusses of S2 fiberglass solid rods and flexures are also feasible. Even so, it was found and should be recognized that there are significant limitations to the approach with current materials. Trusses of solid rods require a significantly greater combination of modulus and strain and the few materials that have these properties (such as nickel-titanium) are not able to operate over the broad range of temperatures encountered in space. In addition, architectures not considered here will certainly require even greater combinations of modulus and strain.

A goal of this work was to develop an understanding of the specific combination of modulus and strain required by concentrated strain structures. Metrics were derived that capture this relationship for trusses. While deployable structures material research has recently focused on developing heat or chemically activated materials that can achieve extremely high strain levels, the metrics and analyses herein show that relatively small strains are required and that passive traditional materials are adequate for many structures. Passive flexure materials with a strain capacity of 3–4% and modulus greater than aluminum (∼70–150 GPa) would enable all of the trusses considered here and likely many other architectures.

Despite the focus of this work on flexure hinge material properties and metrics, one final observation is that reliable failure strain data useful for engineering flexure hinges is rare. The data in Table 1 is derived from standardized American Society for Testing and Materials test methods applied to thick coupons with simple load states. The complex load states of thin flexure hinges strained to 2–4% are not characterized by these tests. In addition to developing new passive materials with greater performance metric values, an area for future research to advance concentrated strain structures is to develop the engineering procedures appropriate to reliably design flexures hinges.

Acknowledgments

This work was funded by the Space Scholars Program at the U.S. Air Force Research Laboratory, Space Vehicles Directorate and a National Science Foundation IGERT fellowship, grant number DGE-0114346.

References

[1] Warren, P. A., Hinkle, J. D., and Harvey, T. J., "Recent Developments in High Efficiency, Elastically Deployed Boom Structures," *44th AIAA Structures, Structural Dynamics, and Materials Conference*, AIAA Paper 2003-1823, April 2003.

[2] Warren, P. A., "Foldable Member," U.S. Patent 6,321,503.

[3] Murphey, T. W., "Chapter 1: Booms and Trusses," *Recent Advances in Gossamer Spacecraft*, edited by H. M. Jenkins, Vol. 212, Progress in Astronautics and Aeronautics, AIAA, Reston, VA, 2006, pp. 1–44.

[4] Mejia-Ariza, J. M., Pollard, E. L., and Murphey, T. W., "Manufacture and Experimental Analysis of a Concentrated Strain Based Deployable Truss Structure," *47th AIAA Structures, Structural Dynamics, and Materials Conference*, AIAA Paper 2006-1686, May 2006.

[5] Pollard, E. L., Murphey, T. W., and Mejia-Ariza, J. M., "Development of Concentrated Strain Based Deployable Truss Structures," *47th AIAA Structures, Structural Dynamics, and Materials Conference*, AIAA Paper 2006-1682, May 2006.

[6] Pollard, E. L., and Murphey, T. W., "Development of Deployable Elastic Composite Shape Memory Alloy Reinforced (DECSMAR) Structures," *47th AIAA Structures, Structural Dynamics, and Materials Conference*, AIAA Paper 2006-1681, May 2006.

[7] Pollard, E. L., Murphey, T. W., and Sanford, G., "Experimental and Numerical Analysis of a DECSMAR Structure's Deployment and Deployed Performance," *48th AIAA Structures, Structural Dynamics, and Materials Conference*, AIAA Paper 2007-2004, April 2007.

[8] Pollard, E. L., Murphey, T. W., and Sanford, G., "Experimental and Numerical Identification of a Monolithic Articulated Concentrated Strain Elastic Structure's (MACSES's) Properties," *48th AIAA Structures, Structural Dynamics, and Materials Conference*, AIAA Paper 2007-2007, April 2007.

[9] Crawford, R., and Benton, M., "Strength of Initially Wavy Lattice Columns," *AIAA Journal*, Vol. 18, No. 5, 1980, pp. 581–584. doi:10.2514/3.50789

[10] Crawford, R., and Hedgepeth, J., "Effects of Initial Waviness on the Strength and Design of Built-Up Structures," *AIAA Journal*, Vol. 13, No. 5, 1975, pp. 672–675.

[11] Crawford, R., "Strength and Efficiency of Deployable Booms for Space Applications," *AAS/AIAA Variable Geometry and Expandable Structures Conference*, AIAA Paper 71-396, April 1971.

[12] Lake, M. S., and Mikulas, M. M., "Buckling and Vibration Analysis of a Simply Supported Column with a Piecewise Constant Cross Section," NASA Technical Paper 3090, March 1991.

L. Peterson
Associate Editor